Molecular Genetics and Metabolism Reports 27 (2021) 100727

Contents lists available at ScienceDirect

Molecular Genetics and Metabolism Reports

journal homepage: www.elsevier.com/locate/ymgmr

The beta-glucuronidase intracisternal A particle insertion model results in similar overall MPSVII phenotype as the single base deletion model when on the same C57BL/6J mouse background

Sean C. Devanney [a], Joseph M. Gibney [a], Colleen G. Le Prell [b], Thomas J. Wronski [c], J.I. Aguirre [c], Issam Mcdoom [d], Coy D. Heldermon [a,*]

[a] College of Medicine, Department of Medicine, University of Florida, Box 100278, Gainesville, FL 32610, United States of America
[b] School of Behavioral and Brain Sciences, University of Texas at Dallas, 1966 Inwood Road, room J216, Dallas, TX 75235, United States of America
[c] College of Veterinary Medicine, Department of Physiological Sciences, University of Florida, Gainesville, FL 32608, United States of America
[d] College of Medicine, Department of Ophthalmology Research, University of Florida, Gainesville, FL 32610, United States of America

ARTICLE INFO

Keywords:
Mouse
Mucopolysaccharidosis VII
Sly syndrome (MPS VII)
Survival
Bone
Retina

ABSTRACT

Two unique gene mutations in the enzyme beta-glucuronidase (GUSB) that result in the lysosomal storage disease Mucopolysaccharidosis (MPS) type VII had previously been reported to have differing disease phenotype severities when compared on differing mouse strains. The MPSVII mouse has proven to be a highly efficacious model to study mucopolysaccharidoses and for evaluating potential gene or stem cell therapies for lysosomal storage diseases. We examined the single base pair deletion (MPSVII) and the intracisternal A particle element insertion (MPSVII2J) in GUSB compared with control animals by skeletal measures, electroretinography, auditory-evoked brainstem response and life span on a C57BL/6J background strain. In all measures, both mutations result in either a trend toward or significant changes from the background strain control. In all measures, there is no significant phenotypic difference between the two mutations. The 2J variant is a more easily genotyped and equally affected phenotype, which holds promise for further studies of chimerism and stem cell therapy approaches.

1. Introduction

MPS type VII is an autosomal recessive disease that results from a deficiency in the enzyme Beta-glucuronidase (GUSB) [1]. GUSB is necessary to degrade chondroitin-4 and -6 sulfates, dermatan sulfate, and heparan sulfate. This leads to the accumulation of these glycosaminoglycans (GAGs) within the lysosomes of many cell types. Cells become increasingly distended with GAGs rendering them ineffectual. Individuals with MPS VII experience a progressive multisystem disease exhibiting coarse facial features, clouding of the cornea, joint stiffness, and developmental regression [2].

MPSVII disease is present in humans and animals, with similar etiologies and pathology [3–8].

The B6.Cg-Gusbmps/BrkJ model, known as MPSVII, has been well characterized and is widely used for studying GUSB deficiencies and has been backcrossed onto the C57BL/6J strain [8]. This strain is a result of a spontaneous mutation resulting in deletion of a single base pair with resulting frameshift and early termination in exon 10 [8]. The genetic sequence of this particular variant prevents the use of quantitative PCR study methods to differentiate the wild type from the mutated gene. Homozygotic MPSVII mice are completely deficient in the enzyme Beta-glucuronidase. The pathology in these mice includes a progressive decrease in hearing [9] and vision [10] along with hepatomegaly and splenomegaly. They phenotypically exhibit short and thickened long bones with a “pug-like” facies. The mouse models quantifiable phenotypic characteristics closely match the human disease course. This has made them very useful as a model for evaluating various potential therapies [11–18].

Another MPSVII mouse model, C3H/HeOuJ-Gusmps-2J, also known as MPSVII2J, arose on the C3H/HeOuJ background strain via an intracisternal A particle element insertion into the 3′ end of intron 8 of GUSB. On the C3H strain the disease phenotype is attenuated [19,20]. On the background C3H strain, baseline GUSB activity is lower than on the B6 background of the B6.Cg-Gusbmps/BrkJ model. The two models had

* Corresponding author.
E-mail address: coy.heldermon@medicine.ufl.edu (C.D. Heldermon).

https://doi.org/10.1016/j.ymgmr.2021.100727
Received 6 October 2020; Received in revised form 28 January 2021; Accepted 29 January 2021

similar low levels of GUSB activity (<1% of normal) in the kidney, liver and spleen but the mean brain GUSB activity was higher in the 2J/C3H. This higher activity was however clarified to reflect one animal in this group and the remaining animals had brain GUSB activity <1%. The 2J/C3H strain had better breeding capacity and longer life span than the B6.Cg-Gusbmps/BrkJ model and seemed to have less relative blunting of bones and limbs. Because of the nature of the mutation in the 2J model, quantitative gene copy numbers would be easier to determine experimentally to discriminate wild type from mutated genes in cells or tissues. The same IAP insertion mutation present on C3H mice has now been backcrossed onto the C57BL/6J mouse background by Dr. Jane Barker. This strain has been evaluated in a Lyme disease and Rheumatoid Arthritis model [21]. Our study examined the effect of each of these two mutations on skeletal, visual, auditory and life span measures. We found that the two mutations confer a similar phenotype when on the same background strain. The 2J variant may be preferable to the GUSB single base pair deletion for evaluation of potential treatment modalities due to the more easily identified PCR amplification product.

2. Materials and methods

2.1. Animals

The pedigreed BL/6 GUSB(MPSVII) mouse strain was acquired from the colony of Dr. Mark Sands (Department of Internal Medicine, Washington University School of Medicine, St. Louis, MO). The pedigreed BL/6 GUSB$^{MPS\text{-}2J}$(MPSVII2J) mouse strain was acquired from Lenny Shultz and Brian Soper at the Jackson Laboratory (Bar Harbor, ME). They were both maintained and expanded in house, by strict sibling mating. Sibling matings were heterozygous (+/−) males crossed with heterozygous (+/−) females. Wild type (+/+), heterozygous (+/−), and mutant (−/−) genotypes were determined by PCR for the MPSVII2J strain and with PCR with restriction enzyme digestion for the BL/6 GUSB (MPSVII) strain per methods outlined by The Jackson Laboratories. The genotypes were confirmed with 4-methylumbelliferyl-beta-D-glucuronide fluorometric assay measuring GUSB activity in collected tissue. All animal procedures were performed in strict accordance with guidelines established by the Institutional Animal Care and Use Committee at the University of Florida in Gainesville, FL.

2.2. Peripheral quantitative computed tomography (pQCT)

The right femurs from male mice were subjected to pQCT analyses with a Stratec XCT Research M instrument (Norland Medical Systems, Fort Atkinson, WI). The distal metaphyseal and diaphyseal scans were performed at 25% and 50% of the length of the femur, respectively. The structural variables that were measured include trabecular bone mineral content (BMC) and bone mineral density (BMD) in the distal femoral metaphysis, and cortical BMD and thickness in the femoral diaphysis. (Normal $n = 5$; MPSVII $n = 4$; MPSVII2J $n = 3$)

2.3. Bone histomorphometry

The distal half of the right femur was processed undecalcified for quantitative bone histomorphometry. The bone samples were sectioned longitudinally at 4 μm thickness with a Leica/Jung 2065 microtome. These sections were stained according to the Von Kossa method with a tetrachrome counterstain. The following variables were measured in the secondary spongiosa of the distal femoral metaphysis: cancellous bone volume, trabecular number, trabecular width, trabecular separation, osteoclast surface, and osteoblast surface. All measurements were performed with the Osteomeasure System (Osteometrics, Decatur, GA).

The pQCT and bone histomorphometric data are presented as the mean ± SEM. These data were analyzed by ANOVA followed by the Holm-Sidak or Dunn's method for pairwise multiple comparisons among the 3 groups. *P* values less than 0.05 were considered to be significant.

2.4. Ex-vivo long bone analysis

Femur lengths: Left and right femurs were collected, cleaned of any remaining soft tissue and measured using calipers for male and female mice >100 days of age at necropsy. They were then fixed and stored in 70% Ethanol until time of bone density analysis (both genders, Normal $n = 8$, MPSVII $n = 9$, MPSVII2J $n = 6$). Lengths were statistically compared by ANOVA using GraphPad Prism v6.

2.5. Behavioral analysis

2.5.1. Electroretinography (ERG)

Vision of mice between 12 and 18 weeks of age, was assessed by electroretinography (ERG) using the UTAS-E 2000 Visual Electrodiagnostic System (LKC). The mice were dark adapted overnight, then anesthetized and pupils dilated. Analysis was first performed under scotopic conditions evaluating rod-mediated responses. Mice were then light-adapted by photobleaching and analyzed under photopic conditions evaluating the cone response. ANOVA for comparison of b wave amplitude was performed. (Normal $n = 12$; MPSVII $n = 9$; MPSVII2J $n = 9$).

2.5.2. Auditory brainstem response (ABR)

Sound-evoked auditory brainstem response (ABR) was measured in 12–18 weeks of age mice at 5, 10, 16, and 32 kHz in the left ear. During ABR tests, animals were anesthetized with ketamine (40 mg/kg, s.c.) and xylazine (8 mg/kg, s.c.) and neural activity in response to brief, tone pips was measured using sterile, 27-gauge electrodes inserted subcutaneously posterior to each pinna and at the vertex of the skull. Tones were generated using TDT System 3 hardware controlled via SigGen software. Levels were decreased from 90 dB SPL to 0 dB SPL in 10-dB increments. Each pip was 10 milliseconds in duration and tones were repeated at a rate of 17/s. Evoked responses were digitally acquired, averaged (1026 responses per frequency x level combination), and stored using BioSig software. Threshold was estimated based on visual inspection of the waveforms by an observer masked to subject genotype. (Normal $n = 15$; MPSVII $n = 9$; MPSVII2J $n = 9$).

2.6. Lifespan

Cohorts of unaffected (+/+ and +/−) BL/6 and mutant (−/−) BL/6 MPSVII and BL/6 MPSVII2J mice were maintained in our animal housing facility under conventional conditions: ambient temperature of 23C, 12-h light/dark cycle, fed a standard diet with access to water ad libitum. Mice were observed daily with individuals used for behavioral studies removed from the housing facility temporarily for the purpose of testing, and promptly returned upon completion of tests. Mice were otherwise undisturbed until their natural death. Experimental mice who died prematurely due to possible complications from anesthesia were censored. All animals were analyzed by Log Rank Mantel-Cox test. A Kaplan-Meier curve was generated to assess survival patterns for the mouse cohorts either with or without mice used for behavioral testing. (Normal $n = 50$; MPSVII $n = 39$; MPSVII2J $n = 37$).

2.7. Statistics

Data analysis was generated using GraphPad Prism 6 (GraphPad Software, La Jolla, CA). ABR analysis was generated using SigmaPlot (Systat Software, San Jose, CA).

3. Results

3.1. Peripheral quantitative computed tomography (pQCT)

The results of the pQCT analyses are shown in Fig. 1. Trabecular BMC in the distal femoral metaphysis (Fig. 1A) was significantly increased by

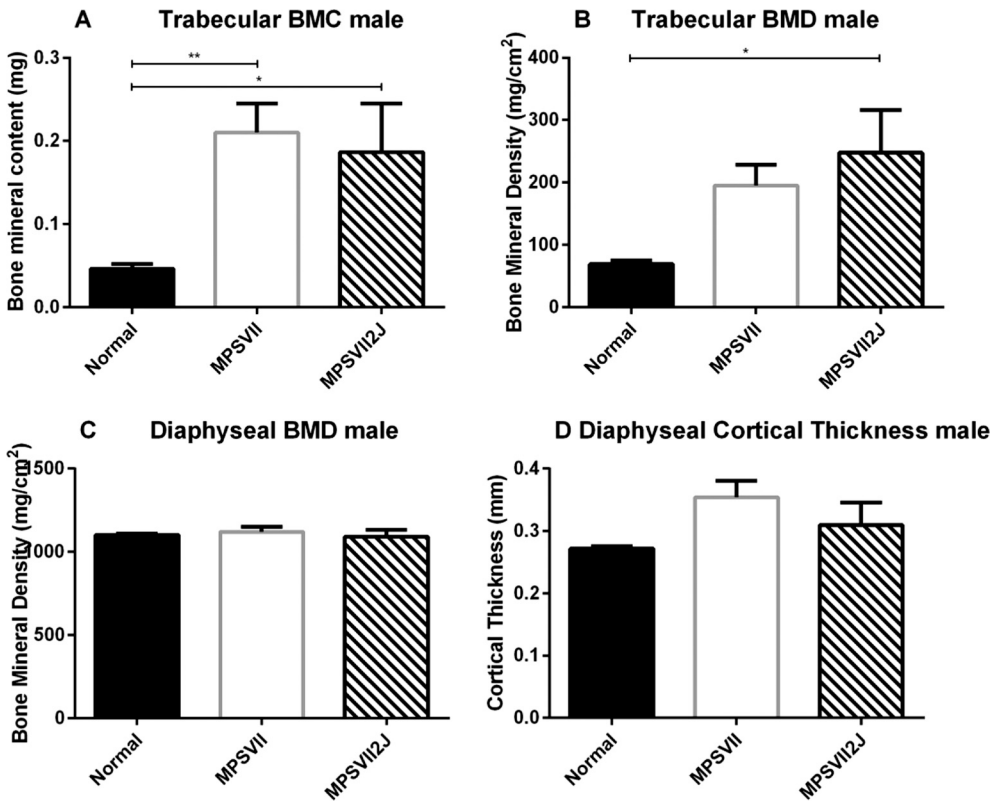

Fig. 1. MPSVII and MPSVII2J mice have increased trabecular mineral content and density than normal controls. Peripheral Quantitative Computed Tomography (pQCT) was performed on right femurs from male mice (Normal $n = 5$; MPSVII $n = 4$; MPSVII2J $n = 3$) at 25% and 50% of the length of the femur, respectively for A trabecular bone mineral content, B trabecular bone mineral density, C diaphyseal bone mineral density and D diaphyseal cortical thickness. * $p < 0.05$, ** $p < 0.01$.

at least a factor of 3 in both the MPSVII and MPSVII2J male mice compared to WT male mice, with no significant difference between the two mutant groups. Trabecular BMD (Fig. 1B) was also significantly increased in the MPSVII2J mice compared to the WT mice. Despite a strong trend for increased trabecular BMD in the MPSVII mice relative to WT mice, statistical significance was not achieved. In the femoral diaphysis, cortical BMD and thickness (Fig. 1C and D) were not significantly increased in the 2 mutant groups compared to the WT group, despite a strong trend for an increase in the latter variable.

3.2. Bone histomorphometry

The results of the bone histomorphometric analysis in the distal femoral metaphysis are shown in Fig. 2. Although both mutant groups exhibited at least 3-fold greater mean values for trabecular bone volume (Fig. 2A) than the WT group, statistical significance was not achieved. However, trabecular separation (Fig. 2B) was significantly decreased in both mutant groups relative to the WT group, and trabecular number (Fig. 2C) was significantly increased in the MPSVII2J mice compared to the WT mice. A strong but nonsignificant trend for increased trabecular number was observed in the MPSVII mice relative to WT mice. Trabecular thickness (Fig. 2D) was not altered by either mutation. Osteoblast surface (Fig. 2E), which is indicative of bone formation, was markedly decreased in both MPSVII and MPSVII2J mice compared to WT mice, although statistical significance was not achieved. Osteoclast surface (Fig. 2F), an index of bone resorption, was not affected by either mutation.

Mean values for all of the above pQCT and bone histo-morpho-metric variables were very similar in the MPSVII and MPSVII2J groups, with no significant differences between them.

Some qualitative differences between mutant and normal mice were apparent in the histologic sections of the distal femur shown in Fig. 3. The growth plates were much wider in both mutant groups compared to the WT group, which is consistent with a previous report in MPSVII mice [15]. Also, osteocyte lacunae were obviously enlarged in cortical and trabecular bone in both mutant groups, and these lacunae appeared to be empty of cellular content.

3.3. Femur lengths

Femur lengths were averaged between left and right femurs in each cohort (Fig. 4). Femurs were significantly shorter for both MPSVII (11.60 ± 0.33 mm; $n = 9$) and MPSVII2J (11.62 ± 0.30 mm; $n = 6$) models, in comparison to normal mice (14.53 ± 0.59; $n = 8$). There was no significant difference of femur lengths between mutant MPSVII and MPSVII2J mice ($P = 0.9998$, Tukey's).

3.4. ERG's

Electroretinography (ERG) tests were performed to verify normal vision in wild-type mice and to gauge deficiencies in the vision of mutant mice as we have previously described [22]. ERG measures the electrical responses of various cell types in the retina. The electrical response to light flashes, eliciting a mixed rod-cone stimulation, was evaluated. We show in Fig. 5 that both the MPSVII and MPSVII2J cohorts have significantly lower visual response at measured frequencies when compared to the normal (+/+ and +/−) mice ($P < 0.0001$). Between 12 and 18 weeks, the visual impairment between both mutant cohorts appears to have deteriorated comparably with no significant difference ($P = 0.7785$).

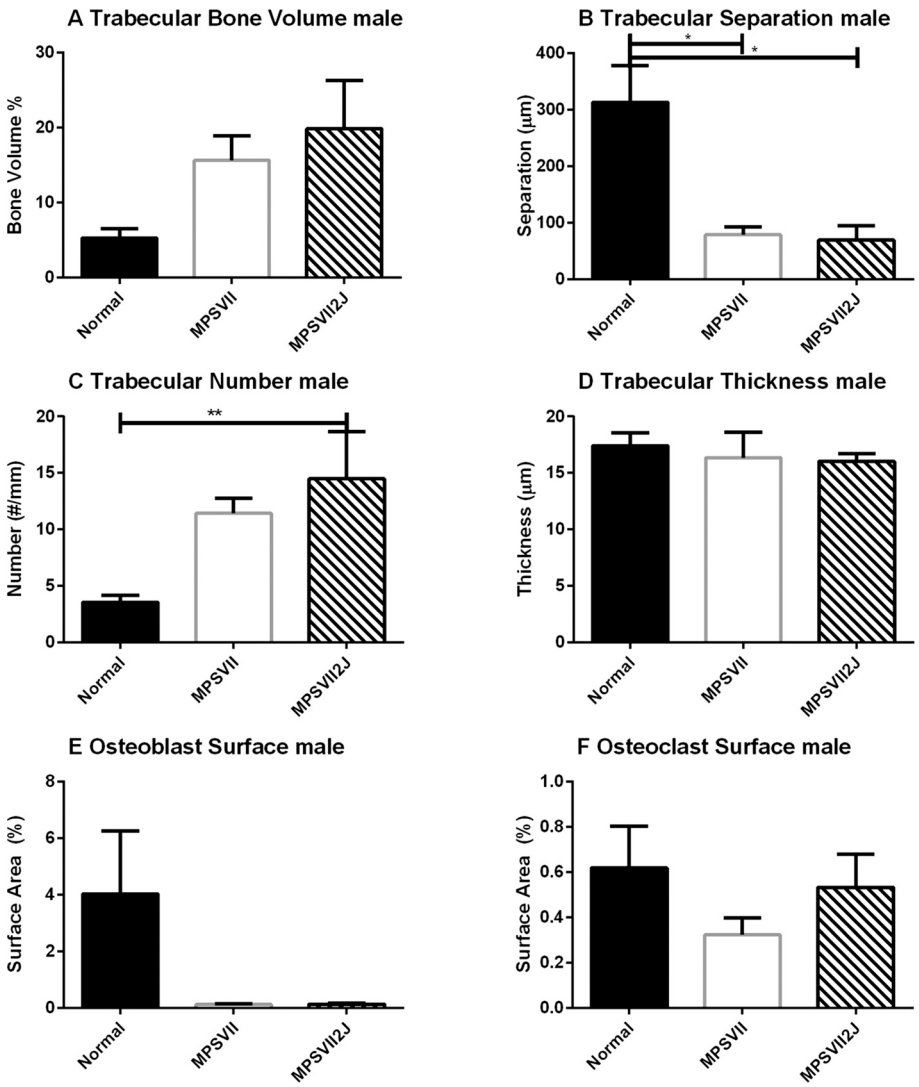

Fig. 2. MPS VII and MPSVII2J mice less trabecular separation and altered osteoblast surface than normal controls. Distal halves of the right femur were processed undecalcified for quantitative bone histomorphometry. Longitudinal bone sections were stained according to the Von Kossa method with a tetrachrome counterstain. The secondary spongiosa of the distal femoral metaphysis was analyzed for A trabecular volume, B trabecular separation, C trabecular number, D trabecular thickness, E osteoblast surface, and F osteoclast surface (Normal $n = 5$; MPSVII $n = 4$; MPSVII2J $n = 3$). All measurements were performed with the Osteomeasure System. * $p < 0.05$, ** $p < 0.01$.

3.5. ABR's

Threshold differences: MPSVII mice. Threshold data collected from the Control mice were compared to the threshold data collected from the MPS VII animals using a two-way Analysis-of-Variance (ANOVA) with genotype (Control, Mutant) and frequency as factors; Bonferroni corrections were used to adjust for multiple pairwise comparisons. There was a significant group difference as a function of genotype ($F = 179.317$, $df = 1,78$; $p \leq 0.001$), with mutants having higher (worse) thresholds than controls. There was also a statistically significant main effect of stimulus frequency ($F = 19.079$, $df = 3,78$; $p \leq 0.001$), with better thresholds at 10 and 20 kHz than at 5 kHz or 32 kHz. There was no reliable interaction between group and frequency; i.e., the effect of genotype on threshold did not vary as a function of which frequency was assessed.

3.5.1. Threshold differences: MPSVII2J mice

Threshold data collected from the Control mice were compared to the threshold data collected from the MPSVII2J animals using a two-way Analysis-of-Variance (ANOVA) with genotype (Control, Mutant) and frequency as factors; Bonferroni corrections were used to adjust for multiple pairwise comparisons. There was a significant group difference as a function of genotype ($F = 34.86$, $df = 1,52$; $p \leq 0.001$), with mutants having higher (worse) thresholds than controls Fig. 6. There was also a statistically significant main effect of stimulus frequency ($F = 6.733$, $df = 3,52$; $p \leq 0.001$), with the best thresholds at 10 kHz. There was no reliable interaction between group and frequency; i.e., the effect of genotype on threshold did not vary as a function of which frequency was assessed.

3.5.2. Threshold differences: MPSVII versus MPSVII2J

Threshold data collected from the MPSVII mutants were compared to the threshold data collected from the MPSVII2J mutants using a two-way Analysis-of-Variance (ANOVA) with genotype (MPSVII, MPSVII2J) and frequency as factors; Bonferroni corrections were used to adjust for multiple pairwise comparisons. The difference in the mean values for the two mutant groups was not large enough to exclude the possibility that the observed differences were due to random sampling variability ($F = 3.585$, $df = 1,71$; $p = 0.063$). The MPSVII mice had thresholds that were elevated by 5–10 dB at each test frequency relative to the MPSVII2J mutants. Although the MPSVII mutants had thresholds that were elevated by 5–10 dB at each test frequency relative to the MPSVII2J mutants, the group difference was not statistically reliable ($t = 2.174$, $p = 0.095$). There was a statistically significant main effect of stimulus frequency ($F = 6.802$, $df = 3,71$; $p < 0.001$), with the best thresholds at 10 kHz. There was no reliable interaction between group and frequency; i.e., the effect of genotype on threshold did not vary as a function of which frequency was assessed.

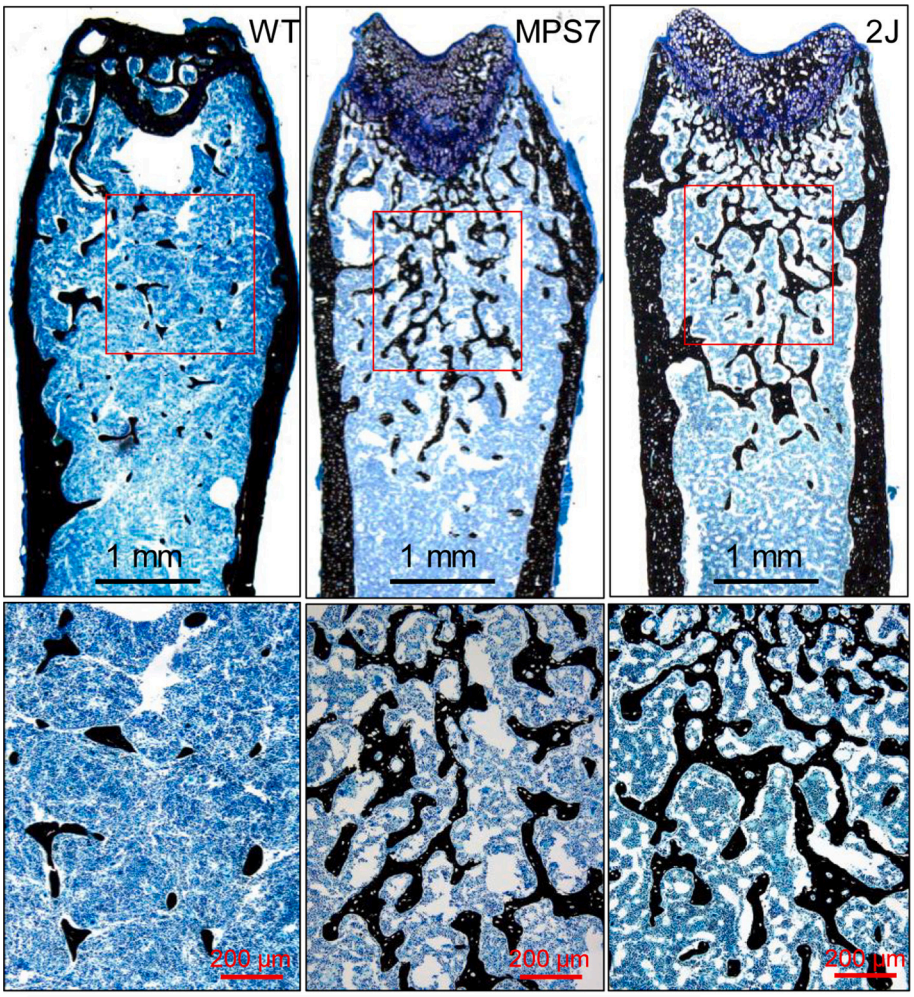

Fig. 3. Histologic photos of the distal femur of wild-type (WT) and MPS7 and 2J mutant mice. Von Kossa stain (black) counterstained with tetrachrome (blue). The increase in trabecular bone mass (black-stained bone) in the mutant mice is obvious. The photos in the lower row depict the metaphyseal areas outlined in red of the upper row photos at a five-fold higher magnification.

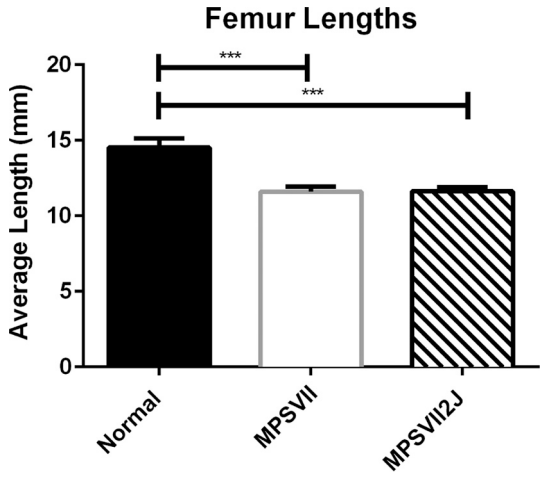

Fig. 4. MPSVII and MPSVII2J mice have shorter femur lengths than normal controls. Femoral length expressed as average length in millimeters between right and left femurs ± SEM (Normal $n = 8$; MPSVII $n = 8$; MPSVII2J $n = 6$). *** $p < 0.001$.

3.6. Life span

We did not find a significant survival difference between the MPSVII and the MPSVII2J mouse cohorts (Fig. 7). Median survival was observed to be 214 ($p = 0.925$ vs MPSVII2J) days for MPSVII and 267 days for MPSVII2J. Both mutant mice strains had deceased one year survival. This is in stark contrast to the unaffected mice cohort with a median survival that was not reached by day 700 with >95% survival (Normal $n = 50$; MPSVII $n = 39$; MPSVII2J $n = 37$).

4. Discussion

In all the comparison studies we carried out, we were only able to observe very small differences between the two MPSVII mutant mouse models on the B6 background. Additionally, these small differences had no statistical significance. This is in contrast to prior studies of these MPSVII mutations when compared on different mouse background strains. When moved to the B6 background, any attenuation of the disease appears to be lost. We believe this indicates that the animal background strain is the primary reason for observed differences as conjectured by previous studies [20,23]. We cannot exclude the possibility of a change in the behavior of the retroposon in the context of the move to the B6 strain. We do observe similar poor breeding behavior for the MPS VII and the MPSVII2J on the B6 background and did not

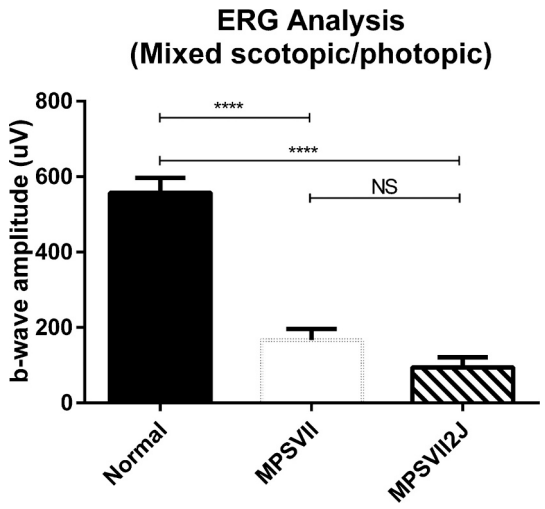

Fig. 5. MPSVII and MPSVII2J mice have diminished light stimulus response than normal controls. ERG analysis of B6- MPSVII and B6- MPSVII2J mice compared to normal B6 mice. A-wave and b-wave amplitudes for both left and right eyes were averaged. The graph is a plot of mixed rod-cone ERG response to stimulus, showing the b-wave amplitude (uV) differences in the three mouse cohorts (Normal $n = 12$; MPSVII $n = 9$; MPSVII2J $n = 9$, $p < 0.0001$). When comparing the MPSVII and MPSVII2J cohorts there is no significant difference ($p = 0.7785$). **** $p < 0.0001$.

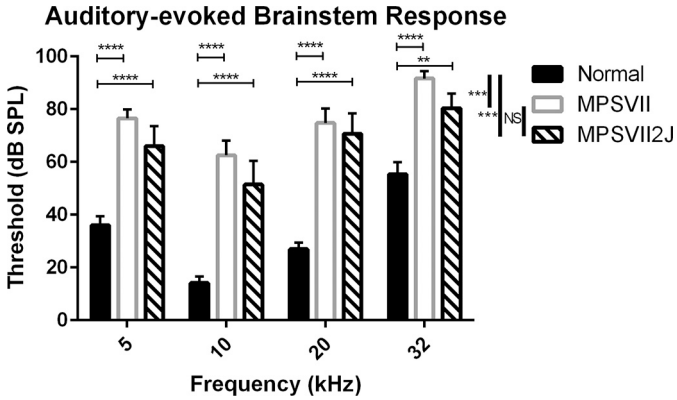

Fig. 6. MPSVII and MPSVII2J mice have diminished audible sensitivity compared to normal controls. Sound-evoked auditory brainstem response (ABR) was measured in 12–18 weeks of age mice at 5, 10, 16, and 32 kHz in the left ear. The dB level at which an auditory evoked brainstem response signal was detectable is shown. (Normal $n = 15$; MPSVII $n = 9$; MPSVII2J $n = 9$, $p < 0.001$). When comparing the MPSVII and MPSVII2J cohorts there is no significant difference. ** $p < 0.01$, *** $p < 0.001$, **** $p < 0.0001$.

observe any difference in enzyme activity on the phenotyping/genotyping samples used to identify mutant animals though we did not carry out extended assays to distinguish 0.1 from 0.3% of normal activity levels.

Regarding the bone phenotype, imaging by pQCT and histomorphometry both indicated that trabecular bone mass was markedly increased in mutant mice. This finding is consistent with a previous report [15]. In addition to bone structural analyses, we also measured % osteoblast and osteoclast surfaces as indices of trabecular bone formation and resorption, respectively. The large decrease in osteoblast surface in both mutant groups indicates that bone formation was suppressed in these mice. In view of this finding, the observed increase

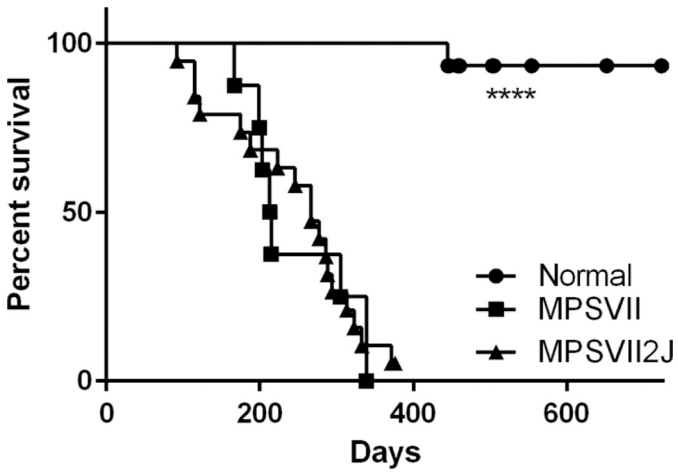

Fig. 7. MPSVII and MPSVII2J mice have shorter lifespans than normal controls. Survival curve by Kaplan-Meier analysis. Both mutant cohorts, MPSVII and MPSVII2J, show similar life-span trends with no significant difference ($P = 0.925$). Both MPSVII ($n = 8$) and MPSVII2J ($n = 19$) populations have a greatly decreased lifespan when compared to normal mice ($n = 15$) ($P < 0.0001$). **** $p < 0.0001$.

in trabecular bone mass in the mutant groups may seem surprising. Although the MPSVII and MPSVII2J mutations did not have a major effect on osteoclast surface, it is important to note that this variable is indicative of osteoclast numbers, not osteoclastic activity. Therefore, the mutations must have inhibited osteoclastic activity in order for an increase in bone mass to occur despite decreased bone formation. This is consistent with prior observations of in vitro bone resorption assays in which MPSVII osteoclasts formed smaller and fewer pits than normal mouse osteoclasts [24]. Furthermore, the decrease in bone resorption must have exceeded the decrease in bone formation for a net gain in bone mass to occur in the mutant mice. This increase in bone mass and decreased bone length has been described previously for the MPSVII mouse model [25]. Importantly, the skeleton responded similarly to the MPSVII and MPSVII2J mutations, and the bone phenotype was nearly identical in these mutant mice.

In contrast to the initial descriptions of the MPSVII2J mouse which demonstrated a markedly attenuated phenotype, the current studies demonstrate that this difference was in all likelihood related to the effect of GUSB deficiency in the context of the C3H background strain. On the C57BL/6 background, morphologically, the MPSVII2J homozygous mouse is similar in appearance to the MPSVII homozygous mouse with similar shortened facies and extremities as demonstrated by equivalent femur lengths in this study. This is consistent with the expected absent GUSB activity of these two mutations. Similarly absent GUSB activity was found in another model, the Gustm(E536A)Sly mouse, and even a small increase in the amount of GUSB activity of 0.1–0.7% resulted in less severe bone morphology and retinal lysosomal distention as was seen in the Gustm(E536Q)Sly and Gustm(L175F)Sly mice [26]. Electroretinography demonstrates that the MPSVII and MPSVII2J mouse models also have equivalently diminished retinal function. Additionally, both models demonstrate similar levels of auditory dysfunction and similar life span. This strongly supports the idea that the genetic background is a major determinant of disease phenotype similar to what is observed in children or siblings with the same mutation demonstrating differing severity of disease phenotype.

5. Conclusions

Our study indicates that the B6·C3-*Gusb*$^{mps\text{-}2J}$/BrkJ (MPSVII2J) model has equivalent functional significance to the B6.Cg-Gusbmps/

BrkJ (MPSVII) model. MPSVII2J has additional potential utility. The large insertion of the IAP element in MPSVII2J may allow for a more robust genotyping and quantitative analysis studies involving transplant or stem cell chimerism investigations.

Acknowledgements

Funding: This work was supported by the National Institutes of Health K08 DK085141 (CDH) & R01NS102624 (CDH) as well as the Gatorade Trust with funds distributed by the University of Florida and has no funding number.

References

[1] W.S. Sly, B.A. Quinton, W.H. McAlister, D.L. Rimoin, Beta glucuronidase deficiency: report of clinical, radiologic, and biochemical features of a new mucopolysaccharidosis, J. Pediatr. 82 (1973) 249–257.
[2] M.F. Coutinho, L. Lacerda, S. Alves, Glycosaminoglycan storage disorders: a review, Biochem. Res. Int. 2012 (2012) 471325, https://doi.org/10.1155/2012/471325.
[3] E.H. Birkenmeier, et al., Murine mucopolysaccharidosis type VII. Characterization of a mouse with beta-glucuronidase deficiency, J. Clin. Investig. 83 (1989) 1258–1266, https://doi.org/10.1172/JCI114010.
[4] D.C. Silverstein Dombrowski, et al., Mucopolysaccharidosis type VII in a German shepherd dog, J. Am. Vet. Med. Assoc. 224 (553–557) (2004) 532–553.
[5] S. Tomatsu, A.M. Montano, V.C. Dung, J.H. Grubb, W.S. Sly, Mutations and polymorphisms in GUSB gene in mucopolysaccharidosis VII (Sly Syndrome), Hum. Mutat. 30 (2009) 511–519, https://doi.org/10.1002/humu.20828.
[6] M.K. Hytonen, et al., A novel GUSB mutation in Brazilian terriers with severe skeletal abnormalities defines the disease as mucopolysaccharidosis VII, PLoS One 7 (2012), e40281, https://doi.org/10.1371/journal.pone.0040281.
[7] P.C. Schultheiss, S.A. Gardner, J.M. Owens, D.A. Wenger, M.A. Thrall, Mucopolysaccharidosis VII in a cat, Vet. Pathol. 37 (2000) 502–505.
[8] M.S. Sands, E.H. Birkenmeier, A single-base-pair deletion in the beta-glucuronidase gene accounts for the phenotype of murine mucopolysaccharidosis type VII, Proc. Natl. Acad. Sci. U. S. A. 90 (1993) 6567–6571.
[9] C.L. Berry, C. Vogler, N.J. Galvin, E.H. Birkenmeier, W.S. Sly, Pathology of the ear in murine mucopolysaccharidosis type VII. Morphologic correlates of hearing loss, Lab Invest 71 (1994) 438–445.
[10] T. Li, B.L. Davidson, Phenotype correction in retinal pigment epithelium in murine mucopolysaccharidosis VII by adenovirus-mediated gene transfer, Proc. Natl. Acad. Sci. U. S. A. 92 (1995) 7700–7704.
[11] B.W. Soper, T.M. Duffy, C.A. Vogler, J.E. Barker, A genetically myeloablated MPS VII model detects the expansion and curative properties of as few as 100 enriched murine stem cells, Exp. Hematol. 27 (1999) 1691–1704.
[12] B.J. Poorthuis, A.E. Romme, R. Willemsen, G. Wagemaker, Bone marrow transplantation has a significant effect on enzyme levels and storage of glycosaminoglycans in tissues and in isolated hepatocytes of mucopolysaccharidosis type VII mice, Pediatr. Res. 36 (1994) 187–193, https://doi.org/10.1203/00006450-199408000-00009.
[13] J.W. Kyle, et al., Correction of murine mucopolysaccharidosis VII by a human beta-glucuronidase transgene, Proc. Natl. Acad. Sci. U. S. A. 87 (1990) 3914–3918.
[14] B.W. Soper, et al., Nonablative neonatal marrow transplantation attenuates functional and physical defects of beta-glucuronidase deficiency, Blood 97 (2001) 1498–1504.
[15] C.E. Macsai, et al., Skeletal response to lentiviral mediated gene therapy in a mouse model of MPS VII, Mol. Genet. Metab. 106 (2012) 202–213, https://doi.org/10.1016/j.ymgme.2012.03.022.
[16] M.S. Sands, et al., Enzyme replacement therapy for murine mucopolysaccharidosis type VII, J. Clin. Invest. 93 (1994) 2324–2331.
[17] J.H. Wolfe, et al., Reversal of pathology in murine mucopolysaccharidosis type VII by somatic cell gene transfer, Nature 360 (1992) 749–753.
[18] A.K. Hennig, et al., AAV-mediated intravitreal gene therapy reduces lysosomal storage in the retinal pigmented epithelium and improves retinal function in adult MPS VII mice, Mol. Therapy J. Am. Soc. Gene Therapy 10 (2004) 106–116.
[19] B. Gwynn, K. Lueders, M.S. Sands, E.H. Birkenmeier, Intracisternal A-particle element transposition into the murine beta-glucuronidase gene correlates with loss of enzyme activity: a new model for beta-glucuronidase deficiency in the C3H mouse, Mol. Cell. Biol. 18 (1998) 6474–6481.
[20] C. Vogler, et al., A novel model of murine mucopolysaccharidosis type VII due to an intracisternal a particle element transposition into the beta-glucuronidase gene: clinical and pathologic findings, Pediatr. Res. 49 (2001) 342–348.
[21] K.K. Bramwell, et al., Lysosomal beta-glucuronidase regulates Lyme and rheumatoid arthritis severity, J. Clin. Invest. 124 (2014) 311–320, https://doi.org/10.1172/JCI72339.
[22] C.D. Heldermon, et al., Development of sensory, motor and behavioral deficits in the murine model of Sanfilippo syndrome type B, PLoS One 2 (2007), e772, https://doi.org/10.1371/journal.pone.0000772.
[23] M.L. Casal, J.H. Wolfe, Variant clinical course of mucopolysaccharidosis type VII in two groups of mice carrying the same mutation, Lab. Investig. J. Tech. Methods Pathol. 78 (1998) 1575–1581.
[24] M.A. Monroy, F.P. Ross, S.L. Teitelbaum, M.S. Sands, Abnormal osteoclast morphology and bone remodeling in a murine model of a lysosomal storage disease, Bone 30 (2002) 352–359, https://doi.org/10.1016/s8756-3282(01)00679-2.
[25] D.J. Rowan, S. Tomatsu, J.H. Grubb, A.M. Montano, W.S. Sly, Assessment of bone dysplasia by micro-CT and glycosaminoglycan levels in mouse models for mucopolysaccharidosis type I, IIIA, IVA, and VII, J. Inherit. Metab. Dis. 36 (2013) 235–246, https://doi.org/10.1007/s10545-012-9522-x.
[26] S. Tomatsu, et al., Missense models [Gustm(E536A)Sly, Gustm(E536Q)Sly, and Gustm(L175F)Sly] of murine mucopolysaccharidosis type VII produced by targeted mutagenesis, Proc. Natl. Acad. Sci. U. S. A. 99 (2002) 14982–14987, https://doi.org/10.1073/pnas.232570999.